IEEE Access
Multidisciplinary | Rapid Review | Open Access Journal

Received May 5, 2020, accepted May 13, 2020, date of publication May 21, 2020, date of current version June 5, 2020.

Digital Object Identifier 10.1109/ACCESS.2020.2996186

MEMS Tunable Frame Antennas Enabling Carrier Aggregation at 600 Mhz

CARLA DI PAOLA[1], (Student Member, IEEE), SAMANTHA CAPORAL DEL BARRIO[1,2], SHUAI ZHANG[1], (Senior Member, IEEE), ARTHUR S. MORRIS III[2], (Fellow, IEEE), AND GERT FROELUND PEDERSEN[1], (Member, IEEE)

[1]Antennas, Propagation and mm-Wave Systems (APMS) Section, Department of Electronic Systems, Aalborg University, 9100 Aalborg, Denmark
[2]WiSpry Inc., Irvine, CA 92618, USA

Corresponding author: Shuai Zhang (sz@es.aau.dk)

This work was supported by the RANGE Project through the Innovation Fund Denmark Together With Industry Partners: WiSpry, AAC, and Sony Mobile.

ABSTRACT The goal of this paper is to propose a tunable antenna system, that aims to cover the LTE low band (699–960 MHz), medium band (1710–2100 MHz) and high band (2100–2690 MHz), as well as the 600 MHz bands by tuning. The architecture consists of four multiband antennas, made up of different radiators, placed in the frame of the mobile handset at the optimized distance of 0.5 mm from each other. Simulations including MEMS tunable capacitors prove that, it is possible to reconfigure the dual resonance in low band, without deteriorating the antennas performance. The tuning ability of the fabricated structure is tested with the PNA and measurements of the total efficiency are performed in the MVG SG24. The results of the measurements are in accordance with the simulations and confirm that the operating frequency of the proposed frame antenna array in low band can be tuned down to the starting point of band 71, with a −6 dB impedance bandwidth of 32 MHz, without altering the antennas behaviour in medium and high band. The resulting peak value of the total efficiency of −5.3 dB at 615 MHz is acceptable, considering the mobile phones in the market. Moreover, the analysis of the user effects, carried out via simulations both in data and in talk mode, reveals a reduced total efficiency of 4 and 8 dB on average, due to the user hand and the user hand-head respectively, compared with the performance in free space.

INDEX TERMS 4G mobile communication, mobile terminal antennas, antenna efficiency, reconfigurable antennas, multifrequency antennas.

I. INTRODUCTION

The standardization of the fourth generation (4G) of mobile communication, featuring long term evolution (LTE) and LTE-advanced technologies allows to provide higher data rates to the users. The enhanced bandwidth, including bands ranging from 699 to 2690 MHz, requires the mobile phone antennas to cover nearly 40 bands in Frequency Division Duplex (FDD) and Time Division Duplex (TDD) [1]. Moreover, considering the low frequency range, beside the frequencies between 699 and 960 MHz, the 600 MHz band (614−698 MHz), previously used for television broadcasting, is also acquired, given the advantages of building penetration and coverage typical of the low bands. Also known as band 71, the 600 MHz Band Plan, shown in Fig. I, includes

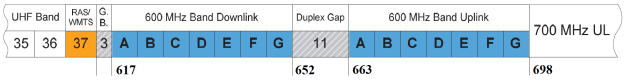

FIGURE 1. The 600 MHz Band Plan [2].

70 MHz of licensed spectrum [2], divided in a downlink band (617 − 652 MHz), an uplink band (663 − 698 MHz), a duplex gap in between (652 − 663 MHz) and a guard band (614 − 617 MHz).

However, the design of handset antennas in low band represents a challenge for antenna engineers, due to the trade-off between size, bandwidth and efficiency [3]. In fact, in order to guarantee the same efficiency, reducing the operating frequency requires to increase the antennas dimensions. Therefore, to the best of our knowledge, tunable antennas result suitable candidates for the low band of 4G mobile phones,

The associate editor coordinating the review of this manuscript and approving it for publication was Hassan Tariq Chattha.

TABLE 1. Gap between frame radiators of mobile phones popular in the last two years.

Brand	Model *	Year	Gap [mm] **
Apple	iPhone X	2017	1
	iPhone 8/8 Plus	2017	2
Samsung	Galaxy S9/S9+	2018	2
	Galaxy S8	2017	2
Huawei	P20 Pro	2018	1.5
	P10/P10 lite	2017	2.5/1.5
	Honor 9	2017	1.5
Nokia	7 Plus	2018	2
OnePlus	6	2018	2

* Mobile phones available at the APMS section.
** Gap measured with a digital caliper with 0.01 mm resolution.

since they are reconfigurable to a wide range of frequencies, while keeping a low profile. A drawback is represented though by the insertion loss of the tuning component. When the antenna resonant frequency is tuned far from the natural value, the quality factor Q increases, generating higher currents on the antenna structure, that flow to the tuners and determine a significant insertion loss, that negatively affects the total efficiency [4], [5].

The contribution of this research work is to implement a tunable handset antenna to address the 600 MHz band, while covering also both low and high frequencies of the 4G spectrum. Therefore, the proposed design employs four antennas in the frame, consisting of radiators working in different bands. The structure presents the advantage over the state-of-the-art frame antennas of a reduced distance of 0.5 mm between adjacent radiating elements, which can still guarantee an acceptable value of the mutual coupling, without using any decoupling structure, as confirmed by the designs in [6]–[12] and the comparison with some of the most popular mobile phones, displayed in Table 1. Moreover, the proposed frame handset antenna gives the benefit of a short clearance, as required for the new generation mobile phones.

Among the alternative techniques to realize frequency tuning proposed in [13]–[15], Micro-Electro-Mechanical Systems (MEMS) tunable capacitors are chosen for the low insertion loss, high voltage handling and very low power consumption [16], as demonstrated in the research efforts in [17]–[21], that make them suitable for tunable antennas to address the 600 MHz band. The antennas system exhibits four resonances in low band, which are independently tunable with four different tuners, in order to optimize the required bandwidth, and multiple resonances in medium and high band, that are not affected by the tuning process, as opposed to [12], [22].

The paper is organized as follows. The design of the structure is presented in Section II. Section III describes the operating principles of the proposed antenna package, showing the analysis conducted on the simulated prototype. Section IV discusses the results of the measurements run on the realized component, comparing them with the results obtained from the simulations. Section V investigates the effect of the user on the antennas performance. Finally, Section VI concludes the paper.

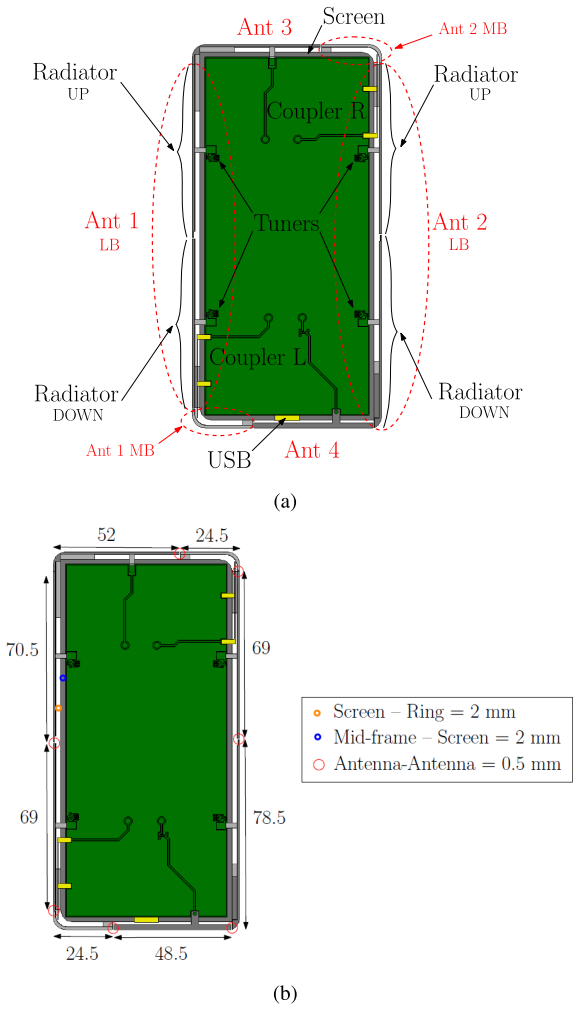

FIGURE 2. Geometric structure and dimensions (mm) of the proposed multiband tunable antennas system for 4G-LTE mobile-phones.

II. SYSTEM CONFIGURATION

A. FRAME ANTENNA STRUCTURE

The proposed antenna package, shown in Fig. 2(a), is made up of four antennas placed symmetrically on the frame. In particular, antennas 1 and 2 are characterized by a coupled structure consisting of a coupler, connected to the feeding line, and three radiators, two vertical, fed by the coupler, that exhibit a dual resonance in low band, and one horizontal, grounded, covering the medium band. Antennas 3 and 4 are two radiators directly fed by the feeding line, working in medium and high band. The dimensions of the antennas are shown in Fig. 2(b), where the short spacing of 0.5 mm between adjacent radiators and the small clearance of 2 mm are highlighted. The entire structure occupies a volume of $158 \times 78 \times 7.5$ mm^3, in order to represent a typical smart-phone form factor, where a 4 layer PCB, made up of three layers of FR-4, with permittivity $\epsilon_r = 4.3$ and loss tangent $\delta = 0.025$, is located inside. The substrates have length 146 mm, width 67 mm and thickness 0.71 mm for the central and 0.36 mm for the top and bottom ones.

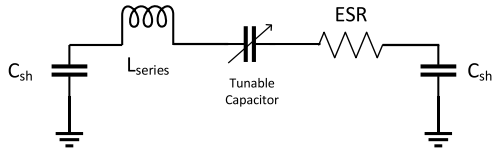

FIGURE 3. Schematic of one bank of a MEMS tunable capacitor [25].

B. CIRCUIT IMPLEMENTATION

Four tuners are embedded in the PCB in order to independently tune the four tunable resonances generated by the low band radiators of antennas 1 and 2 from the 800 MHz region down to band 71. Each tuner consists of four independent Micro-Electro-Mechanical Systems (MEMS) tunable capacitors, provided by *WiSpry* [23], namely the die 1041, described in detail in [24], [25]. The MEMS package contains two banks, each having a series inductance L_{series} of 4.5×10^{-4} nH and a shunt capacitance C_{sh} of 1 pF throughout the operating frequency range, as referred in the schematic representation in Fig. 3. The MEMS tuner exhibits an ESR of 0.2 Ω and Q of 200 at 600 MHz at C_{max}. It presents for each resonance a minimum capacitance $C_{min} = 0.46$ pF, a maximum capacitance $C_{max} = 2.30$ pF and a resolution of 0.0625 pF. Since each of the two low frequency antennas uses two devices, one for each of the two independent resonances, the total tuning range is exploited to tune each resonance from the 800 to the 600 MHz band, while in [22] the two independent banks of the same tuner control each of the two resonances.

The following Fig. 4 shows the circuit implementation of the antennas. In particular, antenna 1 in Fig. 4(a) consists of a coupler connected through a feeding line to the connector, that feeds the two radiators resonating in low frequency. A MEMS tuner is connected to each of them and powered by a battery. The radiator working in medium band is grounded. Moreover, antenna 3 in Fig. 4(b) is directly fed by the feeding line, while for antenna 4 two capacitances, one in series and one in parallel, are needed in order to improve the impedance matching.

III. ANTENNA PERFORMANCE

The structure is analyzed using the electromagnetic simulator *CST Microwave Studio 2019* and the results are presented in the following section. The curves in Fig. 5(a) reproduce the S-parameter characteristics related to the initial and final tuning states of the proposed antenna system, when tuning from 830 to 660 MHz.

A. PERFORMANCE IN THE LOW AND HIGH BANDS OF 4G

The solid lines in Fig. 5(a) represent the state 0, i.e. the natural behaviour of the antenna before the tuning procedure. Antennas 1 and 2 exhibit a dual resonance in low band, resulting from the two vertical radiators. In particular, as proved by the surface current distribution on antenna 1, showed in Fig. 6, the radiator down is responsible of the first resonance and the one up generates the second. In fact, at 760 MHz the

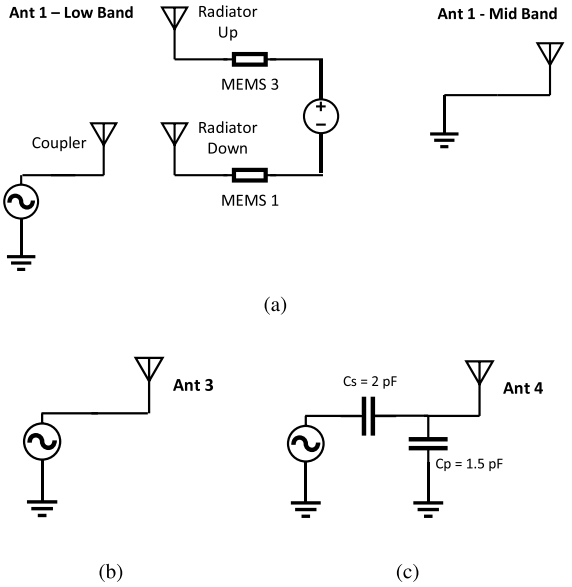

FIGURE 4. Circuit implementation of (a) antenna 1, including low and medium band, (b) antenna 3 and (c) antenna 4. Due to the symmetric structure, antenna 2 is omitted here.

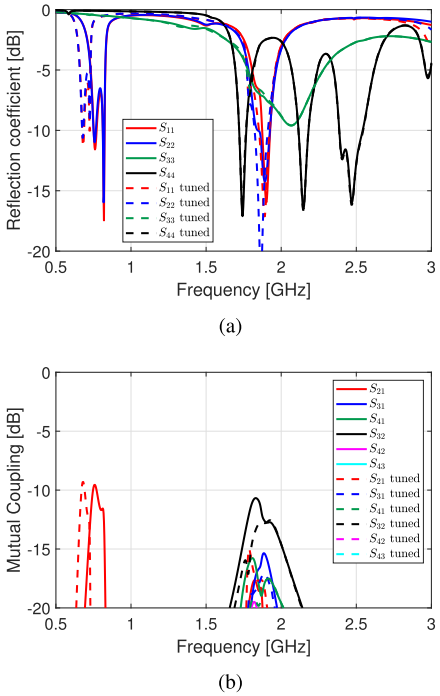

FIGURE 5. Simulated S-parameter characteristics of the proposed antenna package, when tuning from 830 to 660 MHz. (a) Reflection coefficient and (b) mutual coupling of each element.

currents are concentrated on the radiator in the bottom and directed down (Fig. 6(a)), whereas at 820 MHz the currents flow up along the radiator on top (Fig. 6(b)). It is important to highlight that the radiator on top cannot be a standalone resonance, since it is not fed directly, and the same applies to the radiator in the bottom of antenna 2. Both antennas present also a resonance in middle band, due to the third radiator, allowing the overall bandwidth at −6 dB to cover the LTE

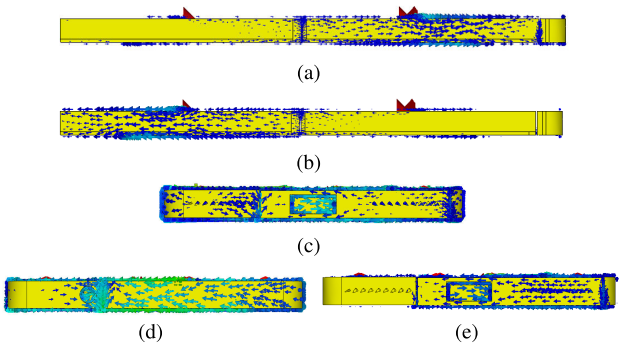

FIGURE 6. Surface current distribution along the frame antennas 1, 3 and 4. In particular (a) the radiator down of antenna 1 at 760 MHz, (b) the radiator up of antenna 1 at 820 MHz, (c) the middle-band radiator of antenna 1 at 1900 MHz, (d) antenna 3 at 2070 MHz and (e) antenna 4 at 2470 MHz.

bands 730 − 830 MHz and 1800 − 1950 MHz. Fig. 6(c) shows the surface currents along the speaker of the middle-band radiator of antenna 1 (radiator on the left) at the resonant frequency of 1900 MHz. Antenna 3 and 4 resonate in middle and high band, where antenna 3 shows a −6 dB impedance bandwidth from 1800 to 2240 MHz, and antenna 4 covers from 1700 to 1800 MHz, from 2100 to 2230 MHz and from 2360 to 2600 MHz. Fig. 6(d) reports a high concentration of currents on antenna 3 at the resonant frequency of 2070 MHz, directed to the jack, placed in the middle-band radiator of antenna 2. Moreover, the opposite direction of the currents on antenna 4 and in the USB port, shown in Fig. 6(e), explains the multiple ripples of S_{44}. The mutual coupling, reported in Fig. 5(b), is acceptable, considering the short separation of 0.5 mm. In fact, further simulations, carried out increasing the width of the gap, prove that the selected value generates a mutual coupling only 1.5 dB higher than the one given by a gap of 2 mm, as shown in Fig. 7(b). In addition, analysing the plot in Fig. 7(a), it results that the smaller gap allows antenna 1 and 2 to cover a bandwidth of 65 MHz, 30 MHz wider than the one achievable with the larger one, making thus the chosen value a good trade off between bandwidth and isolation.

B. PERFORMANCE IN THE 600 MHz-BANDS

The tuning process involves only the low band and does not affect middle and high band, as the dashed lines juxtaposed to the solid lines in Fig. 5(a) prove. The four tuners allow to independently tune the four resonances in order to reach a reasonable compromise between bandwidth and matching. The tuned antennas present a −6 dB impedance bandwidth from 660 to 730 MHz, approximately 20 MHz narrower than the original and with a higher reflection coefficient. The correlation coefficient, reproduced in Fig 8, is lower than 0.5 in the band of interest. From the comparison with the envelope generated before tuning, it is evident that, moving from the original resonant frequency, the curve becomes narrower and higher in value, as for the reflection coefficient.

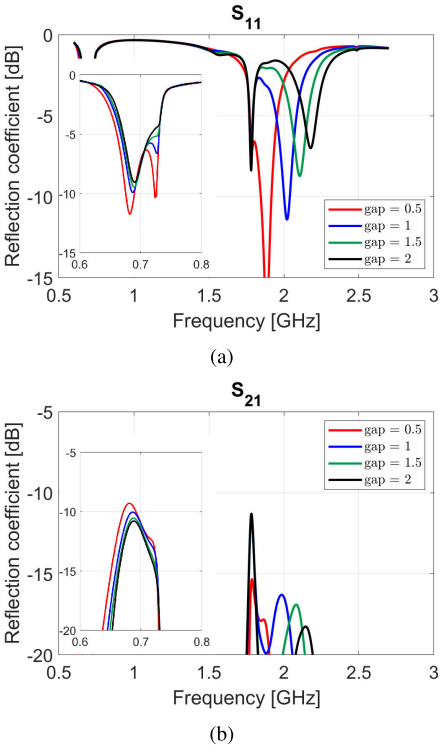

FIGURE 7. Simulated S-parameter characteristics of the proposed antenna package, when increasing the gap from the selected value 0.5 mm to 2 mm. (a) Reflection coefficient and (b) mutual coupling of the most critical elements. Due to the symmetric structure, S_{22} and S_{12} are omitted here.

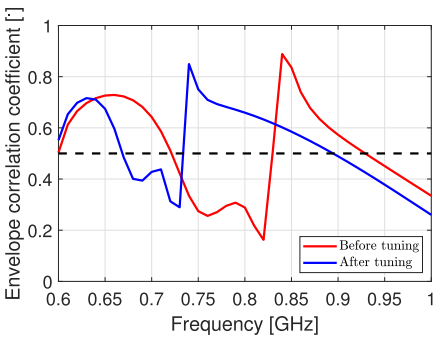

FIGURE 8. Correlation coefficient between antenna 1 and 2, when tuning from 830 to 660 MHz.

IV. MEASUREMENTS RESULTS AND DISCUSSION

The proposed antenna prototype is fabricated and showed in Fig. 9(a), where it is possible to distinguish the main components, the radiators in the frame, connected to the 4 layer PCB through pressure contacts or screw, the two couplers and the four tuners. With the aim to realize a mock-up as realistic as possible, the jack is included on top (Fig. 9(b)) and the speakers and the USB port in the bottom (Fig. 9(c)). In both pictures the small distance of 0.5 mm between adjacent radiators is highlighted. In this section, the description of the tuning system is followed by the discussion of the performance, measured in terms of tuning ability, bandwidth and total efficiency.

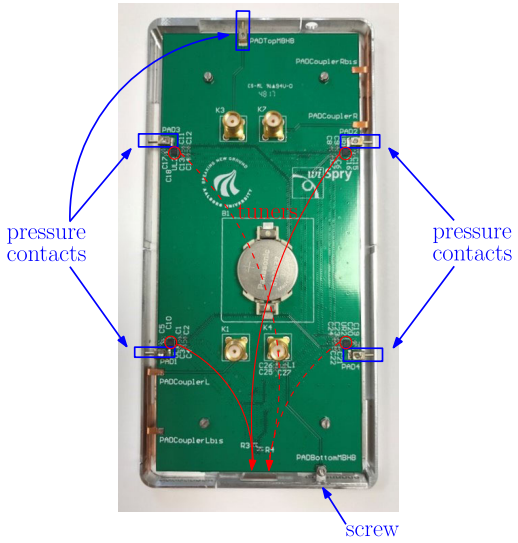

(a)

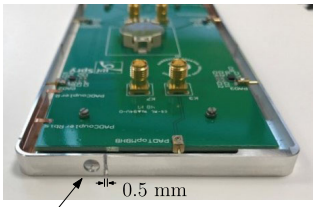

(b)

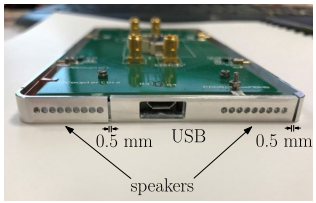

(c)

FIGURE 9. Fabricated frame antennas system and circuitry on the 4 layer PCB. (a) Back view, where the location of the tuners is highlighted (b) top view including the jack, and (c) bottom view, with the speaker and the USB port considered.

A. ANTENNA TUNING

The first step consists in tuning the four MEMS tunable capacitors of each tuner, setting values in the interval from C_{min} to C_{max}, using the software SpryTune provided by WiSpry. In particular MEMS 1 and 2 are programmed with the same values, therefore they are connected to the same exit of the mini USB port (R3), highlighted in Fig. 9(a) with solid red lines. In fact, they tune the first resonances in low band generated by the radiator down of antenna 1 and the radiator up of antenna 2. Same settings are also given to MEMS 3 and 4, to tune the second resonances given by the radiator up of antenna 1 and the radiator down of antenna 2. They are both connected to exit R4, as showed by the dashed red lines in Fig. 9(a). In order to tune antennas 1 and 2 from 840 to the required 617 MHz, the first three tuning states in Table 2 are considered.

B. TEST OF THE TUNING ABILITY

The tunability of the antennas is tested through the evaluation of the S-parameters using the Keysight N5227A Power Network Analyzer (PNA) and the results are presented in Fig. 11. They confirm what is observed in the simulations, i.e. tuning the low band does not influence the middle and high band, therefore a zoom in the low band is chosen to better evaluate each tuning state. Moreover, from a general overview of the plots, it is possible to notice that the bandwidth shrinks, when the antenna is tuned far from the natural resonant frequency, and the reflection coefficient becomes higher. Accurate details about the achievable -6 dB impedance bandwidth are reported in Table 3, which highlights that, at the last state, state 3, the bandwidth is one third of its value at the initial state, but relatively wide, considering that the resonance is tuned approximately 130 MHz down. Even though not required by the specifications, the tuners allow to tune towards lower frequencies, outside band 71, reaching 500 MHz, and this final state is still able to guarantee a -6 dB impedance bandwidth of 17 MHz. For all the configurations analyzed the measured mutual coupling is less than -10 dB, reporting a good agreement between simulations and measurements.

In Fig. 12(a) the curves related to the three required tuning stages are juxtaposed to point out the gradual bandwidth reduction, as the operating frequency decreases, and to show the complete overlapping of the curves in middle band, which are not affected by the tuning.

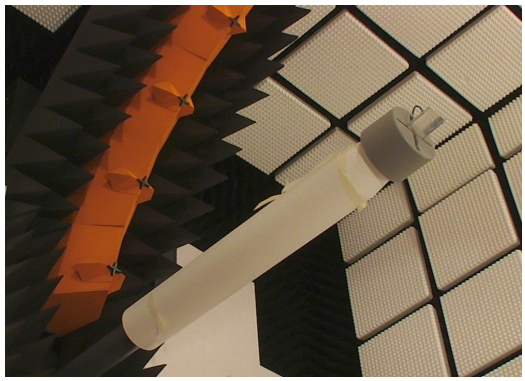

FIGURE 10. Demonstrator in the measurement facility, the MVG SG24.

TABLE 2. MEMS tuner settings for antenna 1 *.

States	Tuner 1 [pF]	Tuner 2 [pF]
State 0	$C_{min} = 0.46$	$C_{min} = 0.46$
State 1	0.5	1.2
State 2	1.3	1.7
State 3	2.4	2.5
State max	$C_{max} = 6.6$	$C_{max} = 6.6$ **

* Due to the symmetric structure, the tuner settings for antenna 2 are omitted here.
** C_{max} refers to the whole chip, i.e. both banks at maximum capacitance (outside the requirements).

TABLE 3. Measured bandwidths of Fig. 11 and efficiencies of Fig. 13(a).

Tuning State	-6 dB Bandwidth [MHz]	Efficiency [dB]
State 0	$740 - 838$ (~ 98)	-3.1
State 1	$700 - 762$ (~ 62)	-3.3
State 2	$650 - 696$ (~ 46)	-5.4
State3	$614 - 646$ (~ 32)	-5.3
State max	$500 - 517$ (~ 17)	N.A. *

* Calibration not available in the corresponding frequency range.

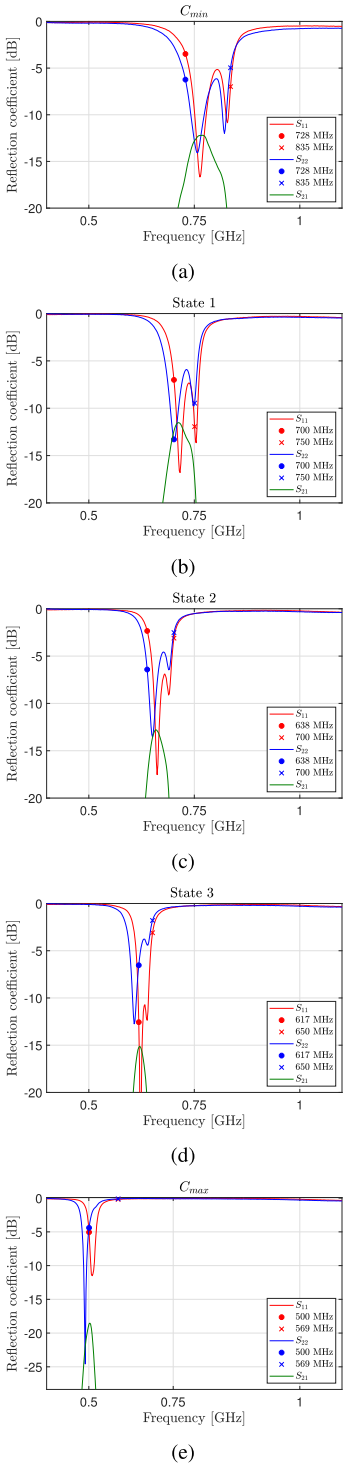

FIGURE 11. Measured return loss in low band in the tuning stages referred in Table 2. (a) State 0 with tuners at C_{min}, (b) State 1, (c) State 2, (d) State 3 and (e) State *max* with tuners at C_{max}.

Finally, Fig. 12(b) contains the frequency response of the whole antennas system, after tuning antennas 1 and 2 down to 617 MHz, where it is possible to notice the difference between antennas 3 and 4, despite their symmetry. The matching problems reported by antenna 4 are due to the presence of the USB port, responsible of the ripples already observed

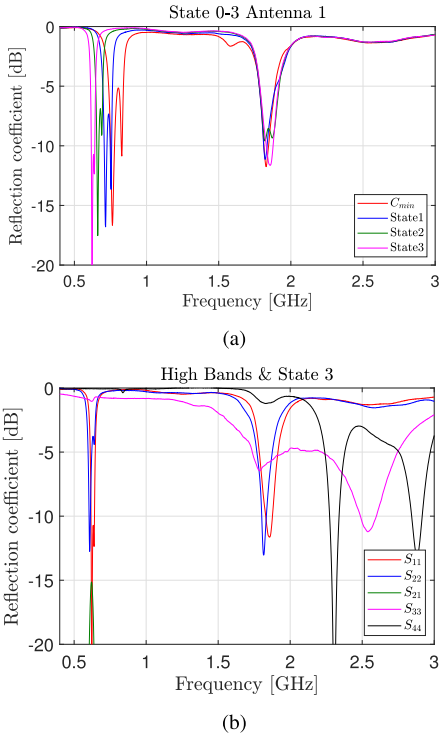

FIGURE 12. Measured return loss of (a) antenna 1 including middle band in different tuning stages and (b) the whole antennas system, after tuning the low band to the desired frequency.

in the simulations. In fact, the microphone has a negligible effect, as for the jack for antenna 3.

C. EVALUATION OF THE TOTAL EFFICIENCY

In order to evaluate the achievable efficiency of the proposed antenna design in the low bands of 4G, measurements are performed in the MVG SG24 located in the laboratory of the Antennas, Propagation and Millimeter-Wave Systems (APMS) section at Aalborg University. The measurements setup consists of a ring with 23 bi-directional and dual polarized test probes and a computer receiving the measured data from the device under test. The antenna under test (AUT) is suitably positioned in the center of the ring, as shown in Fig. 10, where it is possible to see the edge-to-edge screen in aluminium. The total efficiency is computed with 3D pattern integration technique and the results for antennas 1 and 2 in the tuning stages are shown in Fig. 13(a). Despite their symmetry, antennas 1 and 2 exhibit a different efficiency, higher for antenna 2 at the last two tuning states, possibly due to manufacturing errors. As expected, the efficiency decreases, when the antennas are tuned far from their natural resonance, as a significant amount of current flows to the tuners, causing a higher insertion loss. At the third state the maximum total efficiency is -5.3 dB, as registered in Table 3, which is an acceptable value in low band, considering the state-of-the-art mobile phones [26]. Finally, in Fig. 13(b), the total efficiency is plotted for the four antennas in the corresponding working bands. Once again, it is possible to notice how the matching components degrade the performance of

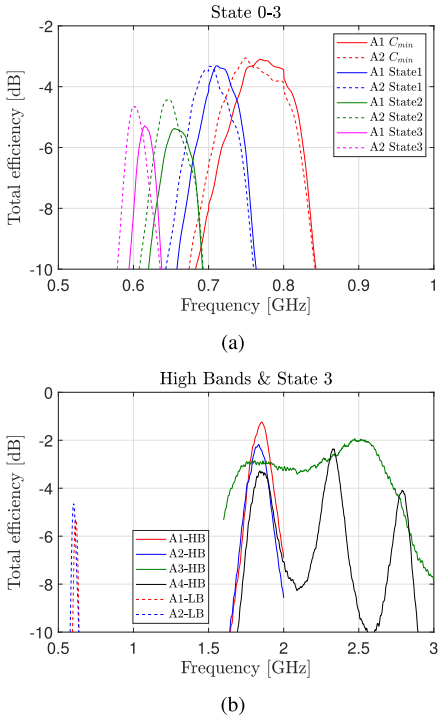

FIGURE 13. Measured efficiency of (a) antennas 1 and 2 in different tuning stages and (b) the four antennas in the corresponding working bands, after tuning the low band to the desired frequency. The curves plotted include also 0.2 – 0.5 dB trace loss.

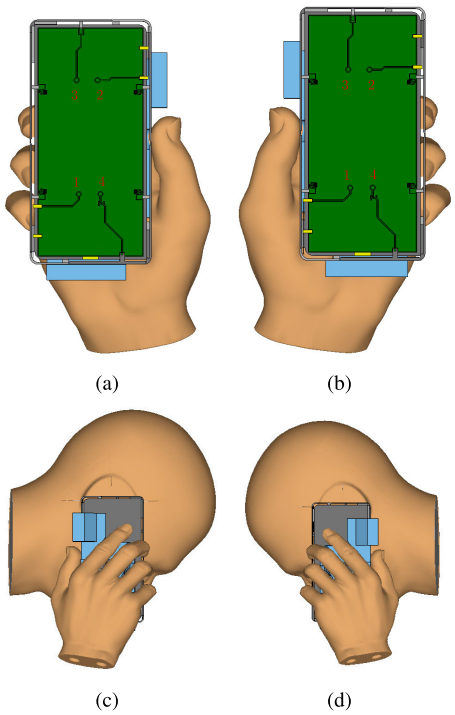

FIGURE 14. Simulations setup to evaluate the impact of the user. Data mode, including (a) right and (b) left hand phantoms, and talk mode with (c) right and (d) left hand next to head phantom.

antenna 4, whose total efficiency is lower than −10 dB at 2.6 GHz.

V. USER EFFECTS

A. BODY LOSS

The evaluation of the impact of the user on the performance of the frame antenna array is conducted in terms of total efficiency, calculated through simulations including a phantom hand in data mode and the phantom hand next to a phantom head in talk mode. Figure 14 shows the setups simulated in CST, where both right and left hand grip are considered. The simulated hands and specific anthropomorphic mannequin (SAM) head represent the prototypes used for the measurements, which are in accordance with the CTIA specifications [27].

First, in Fig. 15, the curves representing the return loss of each antenna in the four user cases are juxtaposed with that in free space. In general, they point out that the impedance matching is more affected by the user hand, whereas negligible effects are given by the head. At low band, considering antenna 1 in Fig. 15(a), the right hand grip causes more significant mismatch loss and detuning compared to the left hand, meaning that the thumb has a minor influence than the last three fingers. Nevertheless, the detuning can be compensated, since the proposed antenna is frequency-reconfigurable. Opposite considerations apply to antenna 2, whose reflection coefficients are shown in Fig. 15(b). Looking at the middle band, the left hand grip is more responsible for the mismatch of both antennas, particularly of antenna 1. Considering middle and high band, antenna 3 in Fig. 15(c) suffers from a shift of 100 MHz backward of the resonance frequency in all the user's configurations. The effects on antenna 4 are more significant at 2.5 GHz, as proved in Fig. 15(d) and can be especially attributed to the touch of the palm of the right hand.

The total efficiency of the four antennas is reported in the bands of interest in Fig. 16, where the performance in the four different user scenarios are compared with the free space. Considering antenna 1 at 660 MHz (Fig. 16(a)), the simulation with right and left hand yield a total efficiency of −9.5 and −7 dB respectively, versus −4 dB in free space. Moreover, the simulations of the talk mode show a total efficiency 3 – 4 dB lower than the corresponding data mode. This values are in accordance with typical absorption loss due to the presence of the user [28]. By contrast, the total efficiency of antenna 2 (Fig. 16(b)) is higher in the right hand data mode and corresponding talk mode, as expected. Better values of the total efficiency are gathered in middle band, except for the configurations with left hand grip related to antenna 1, due to the mismatch highlighted in Fig. 15(a). However, when antenna 1 is affected by lower efficiency, implementing the diversity function allows to select antenna 2 and vice versa.

Concerning antenna 3, it is evident from Fig. 16(c) that both hands phantoms have a negligible impact on the total efficiency, since they do not interfere with the radiation. On the other hand, the presence of the head in talk mode decreases the performance by 5 dB on average.

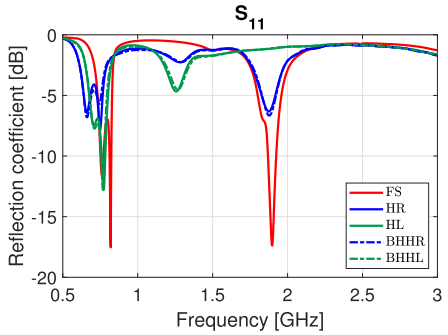

(a)

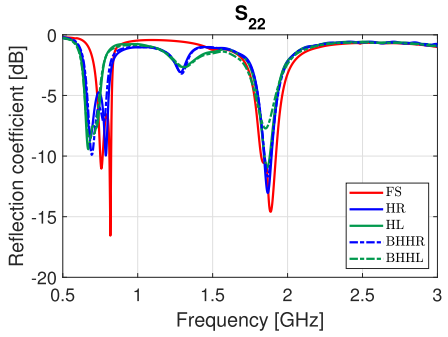

(b)

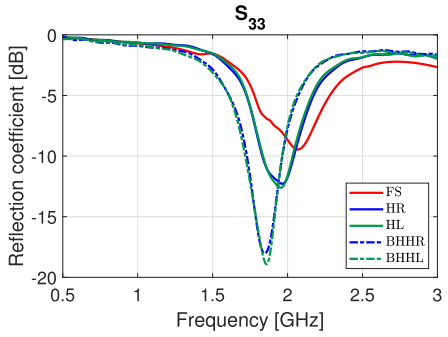

(c)

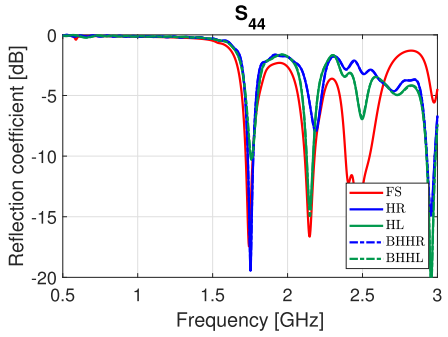

(d)

FIGURE 15. Comparison of the return loss of antenna (a) 1, (b) 2, (c) 3 and (d) 4 when in free space (FS), in data mode hold by right hand (HR) and left hand (HL), and in talk mode in the configurations beside hand and hand right (BHHR) and beside head and hand left (BHHL).

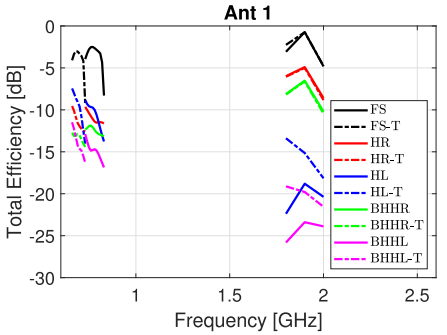

(a)

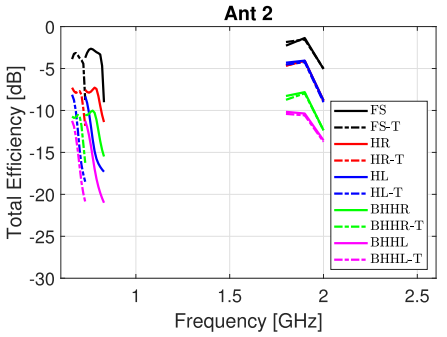

(b)

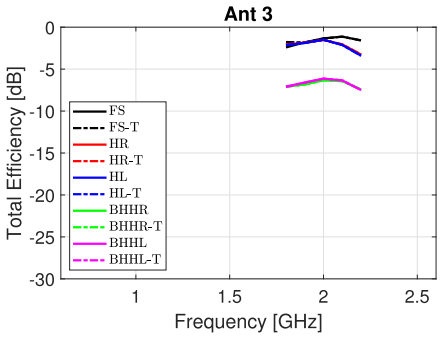

(c)

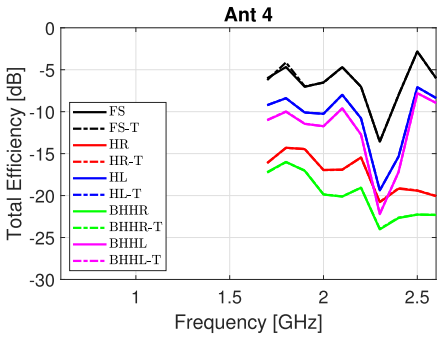

(d)

FIGURE 16. Comparison of the total efficiency of antenna (a) 1, (b) 2, (c) 3 and (d) 4 when in FS, hold by the user hand phantom in data mode and in the presence of the user hand and head phantoms in talk mode. For all the configurations, the results before and after tuning (T) are plotted.

The same comments valid for the return loss of antenna 4 apply to the results plotted in Fig. 16(d). The reduction of the total efficiency, when the phone is held with the right hand, is due to the palm that covers the antenna and obstructs the radiation.

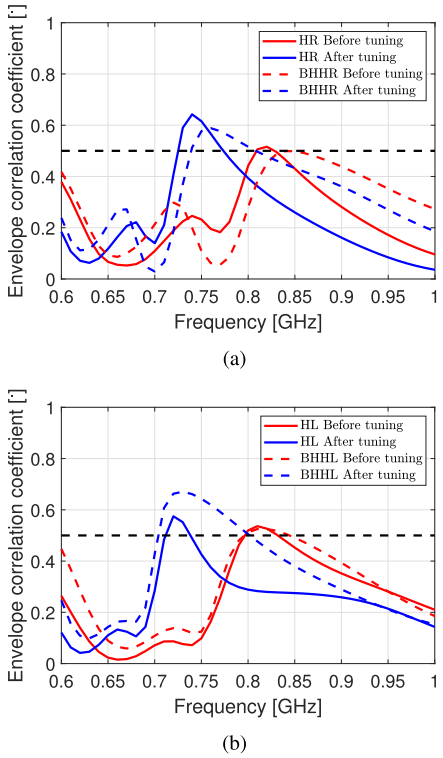

FIGURE 17. User impact on the correlation coefficient between antenna 1 and 2, when tuning from 830 to 660 MHz. (a) Data mode hold by right hand (HR) and talk mode beside hand and hand right (BHHR), (b) data mode hold by left hand (HL) and talk mode beside hand and hand left (BHHL).

Figure 17 reports the envelope correlation coefficient between antenna 1 and 2 in data mode and talk mode. From the comparison with the results in free space, shown in Fig. 8, it is possible to notice that the impact of the user decreases the correlation, that is lower than 0.5 in a wider bandwidth. As expected, the curves generated after tuning are narrower than the corresponding ones before tuning also in the four user cases. However, the value of the correlation coefficient does not increase significantly after tuning, as opposed to the behavior in free space.

Finally, the influence of the user on the radiation characteristics of each antenna is investigated in data mode and talk mode and compared with the performance in free space in Fig. 18, in order to corroborate the previous discussion. The radiation pattern of antenna 1 remains unaltered throughout the tuning stages, therefore only the results at 680 MHz are included in Fig. 18(a). Analyzing the effects of the hand grip, it is possible to notice that the fingers of the right hand flip the pattern towards the front, whereas the thumb of the left hand slightly tilts it. Moreover, when bringing the system close to the right ear, the head fully reflects the pattern, but it directs it to the bottom of the neck, if the device is placed on the left side. Same considerations apply to antenna 2 in the opposite hand and side of the head.

Looking at the results of antenna 3 at the resonance frequency of 2070 MHz in Fig. 18(b), both hands do not alter the direction of the main beam. On the other hand, when the

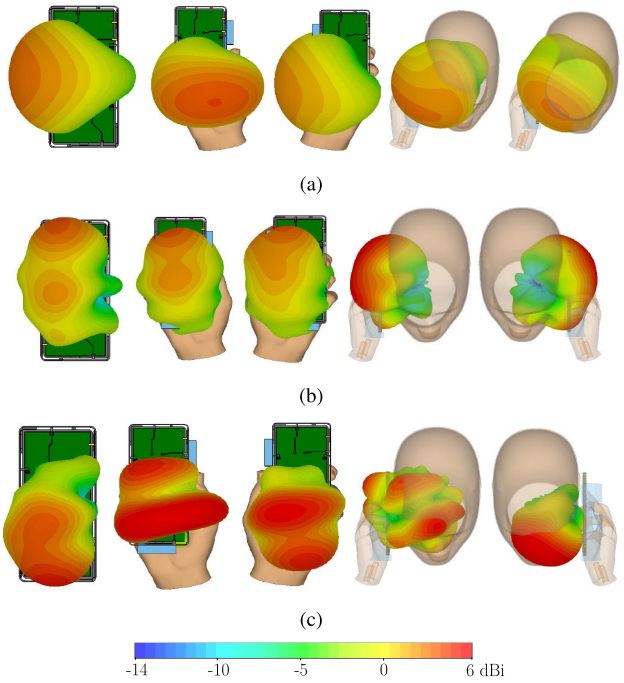

FIGURE 18. Directivity of antenna (a) 1, (b) 3, (c) and 4 when in free space, hold by the user hand phantom in data mode and in the presence of the user hand and head phantoms in talk mode.

TABLE 4. Simulated specific absorption rate (SAR) (Units:W/kg).

Antenna	Frequency [GHz]	Right Side	Left Side
Ant 1	0.68	0.54	0.58
	0.72	1.32	0.81
	0.76	0.48	0.59
	0.82	0.55	0.42
	1.9	0.44	1.37
Ant 2	0.68	0.34	0.75
	0.72	0.32	0.6
	0.76	0.43	0.74
	0.82	0.37	0.44
	1.9	0.5	1.07
Ant 3	2.1	1.43	1.42
Ant 4	2.1	0.19	0.15

antenna touches the ears in talk mode, the beam is reflected externally.

As mentioned above, the palm of the hands has a significant impact on the radiation pattern of antenna 4, evaluated at 2470 MHz and shown in Fig. 18(c). Moreover, a large difference can be observed between the two placements in talk mode. In fact, on the right side the pattern results totally distorted, while the main beam is restored on the left side.

B. SPECIFIC ABSORPTION RATE

The specific absorption rate (SAR) is a measure of the user exposure to the electromagnetic fields. Considering 23 dBm accepted input power for LTE frequencies, the resulting SAR must be below 1.6 W/kg over 1 g mass of tissue [29]. The values reported in Table 4 for the four frame antennas, evaluated both at the right and left side of the SAM head with the DUT in cheek position, meet the SAR

specifications for commercial phones. The highest values are registered for antenna 1 and 2 in middle band, when the phone is placed on the left side of the head, and for antenna 3 the SAR reaches 1.4 W/kg on both sides at 2.1 GHz.

VI. CONCLUSION

This work proposes the design of a tunable antenna array to cover the LTE spectrum, with particular focus on the 600 MHz band. The proposed architecture consists of four multiband antennas on the frame and is equipped with MEMS tunable capacitors, that have the function to lower the natural resonant frequency to the desired point. The simulated component exhibits good performance in terms of bandwidth and mutual coupling, that maintains an acceptable value, despite the reduced distance between the radiating elements. The structure is manufactured and the tunability is tested with the PNA. The results demonstrate that three tuning states are required for the antenna system to resonate at the starting point of band 71 and report a relatively wide -6 dB impedance bandwidth of 32 MHz. The same behaviour is shown in middle and high band. The measurements conducted in the MVG SG24 report a total efficiency of -5.3 dB at 615 MHz, which is in line with the mobile phones in the market. Moreover, the effect of the user's hand and head on the total efficiency is investigated through simulations and comparison of three different scenarios, free space, data mode and talk mode. As expected, the hand grip generates mismatching and detuning to different degrees to the four antennas. Concerning the impact on the total efficiency, a reduction of 4 dB on average is observed in data mode in comparison to the free space and a further decrease of 4 dB is evaluated when the device is placed in talk mode. Future work aims to improve the design of the frame antenna array, taking into account the user influence, in order to cope with the drastic reduction of the performance, once the device is used in the real scenario.

REFERENCES

[1] *Feasibility Study for Further Advancements for E-Utra (LTE-Advanced)*, Standard ETSI TR 136 912, 2012.
[2] *Incentive Auction Closing and Channel Reassignment Public Notice; Incentive Auction Closes; Reverse Auction and Forward Auction Results Announced; Final Television Band Channel Assignments Announced; Post-Auction Deadlines Announced*, Federal Communications Commission, Washington, DC, USA, Apr. 13, 2017.
[3] R. F. Harrington, "Effect of antenna size on gain, bandwidth, and efficiency," *J. Res. Nat. Bureau Standards*, vol. 64D, no. 1, pp. 1–12, Jan./Feb. 1960.
[4] A. D. Yaghjian and S. R. Best, "Impedance, bandwidth, and q of antennas," *IEEE Trans. Antennas Propag.*, vol. 53, no. 4, pp. 1298–1324, Apr. 2005.
[5] J. S. McLean, "A re-examination of the fundamental limits on the radiation q of electrically small antennas," *IEEE Trans. Antennas Propag.*, vol. 44, no. 5, p. 672, May 1996.
[6] W.-C. Wu and K.-L. Wong, "Metal-frame inverted-f antenna for the LTE metal-casing smartphone," in *Proc. Int. Symp. Antennas Propag. (ISAP)*, Oct. 2016, pp. 288–289.
[7] H. Chen and A. Zhao, "LTE antenna design for mobile phone with metal frame," *IEEE Antennas Wireless Propag. Lett.*, vol. 15, pp. 1462–1465, 2016.
[8] I. R. R. Barani and K.-L. Wong, "Integrated Inverted-F and open-slot antennas in the metal-framed smartphone for 2×2 LTE LB and 4×4 LTE M/HB MIMO operations," *IEEE Trans. Antennas Propag.*, vol. 66, no. 10, pp. 5004–5012, Oct. 2018.
[9] J. Choi, W. Hwang, C. You, B. Jung, and W. Hong, "Four-element reconfigurable coupled loop MIMO antenna featuring LTE full-band operation for metallic-rimmed smartphone," *IEEE Trans. Antennas Propag.*, vol. 67, no. 1, pp. 99–107, Jan. 2019.
[10] D. Huang, Z. Du, and Y. Wang, "Eight-band antenna for full-screen metal frame LTE mobile phones," *IEEE Trans. Antennas Propag.*, vol. 67, no. 3, pp. 1527–1534, Mar. 2019.
[11] K.-L. Wong and Y.-C. Wu, "Small-size dual-wideband IFA frame antenna closely integrated with metal casing of the LTE smartphone and having decreased user's hand effects," *Microw. Opt. Technol. Lett.*, vol. 58, no. 12, pp. 2853–2858, Dec. 2016.
[12] K.-L. Wong and C.-Y. Tsai, "Half-loop frame antenna for the LTE metal-casing tablet device," *IEEE Trans. Antennas Propag.*, vol. 65, no. 1, pp. 71–81, Jan. 2017.
[13] L. Huang and P. Russer, "Electrically tunable antenna design procedure for mobile applications," *IEEE Trans. Microw. Theory Techn.*, vol. 56, no. 12, pp. 2789–2797, Dec. 2008.
[14] J. T. Bernhard, "Reconfigurable antennas," *Synth. Lect. Antennas*, vol. 2, no. 1, pp. 1–66, 2007.
[15] S. Caporal Del Barrio, M. Pelosi, G. F. Pedersen, and A. Morris, "Challenges for frequency-reconfigurable antennas in small terminals," in *Proc. IEEE Veh. Technol. Conf. (VTC Fall)*, Sep. 2012, pp. 1–5.
[16] N. Haider, D. Caratelli, and A. G. Yarovoy, "Recent developments in reconfigurable and multiband antenna technology," *Int. J. Antennas Propag.*, vol. 2013, pp. 1–14, Mar. 2013.
[17] Q. Gu and J. R. De Luis, "RF MEMS tunable capacitor applications in mobile phones," in *Proc. 10th IEEE Int. Conf. Solid-State Integr. Circuit Technol.*, Nov. 2010, pp. 635–638.
[18] J. Ilvonen, R. Valkonen, J. Holopainen, and V. Viikari, "Multiband frequency reconfigurable 4G handset antenna with mimo capability," *Prog. Electromagn. Res.*, vol. 148, pp. 233–243, 2014.
[19] E. Erdil, K. Topalli, M. Unlu, O. A. Civi, and T. Akin, "Frequency tunable microstrip patch antenna using RF MEMS technology," *IEEE Trans. Antennas Propag.*, vol. 55, no. 4, pp. 1193–1196, Apr. 2007.
[20] D. E. Anagnostou, G. Zheng, M. T. Chryssomallis, J. C. Lyke, G. E. Ponchak, J. Papapolymerou, and C. G. Christodoulou, "Design, fabrication, and measurements of an RF-MEMS-Based self-similar reconfigurable antenna," *IEEE Trans. Antennas Propag.*, vol. 54, no. 2, pp. 422–432, Feb. 2006.
[21] G. H. Huff and J. T. Bernhard, "Integration of packaged RF MEMS switches with radiation pattern reconfigurable square spiral microstrip antennas," *IEEE Trans. Antennas Propag.*, vol. 54, no. 2, pp. 464–469, Feb. 2006.
[22] S. Caporal del Barrio, E. Foroozanfard, A. Morris, and G. F. Pedersen, "Tunable handset antenna: Enhancing efficiency on TV white spaces," *IEEE Trans. Antennas Propag.*, vol. 65, no. 4, pp. 2106–2111, Apr. 2017.
[23] *WiSpry*. Accessed: Feb. 25, 2020. [Online]. Available: http://wispry.com/solutions/tunable-digital-capacitor-arrays/
[24] S. Caporal Del Barrio, A. Morris, and G. F. Pedersen, "MEMS tunable antennas: Reaching for the 600 MHz-bands," in *Proc. IEEE-APS Topical Conf. Antennas Propag. Wireless Commun. (APWC)*, Aug. 2014, pp. 1–4.
[25] S. Caporal del Barrio, J. Hejselbak, A. Morris, and G. F. Pedersen, "Combining antenna and ground plane tuning to efficiently cover tv white spaces on handsets," in *Proc. 11th Eur. Conf. Antennas Propag. (EUCAP)*, Mar. 2017, pp. 2964–2968.
[26] A. Tatomirescu and G. F. Pedersen, "Body-loss for popular thin smart phones," in *Proc. 7th Eur. Conf. Antennas Propag. (EuCAP)*, Apr. 2013, pp. 3754–3757.
[27] *Test Plan for Wireless Device Over-the-Air Performance*, CTIA, Washington, DC, USA, Nov. 2016.
[28] M. Pelosi, O. Franek, M. B. Knudsen, M. Christensen, and G. F. Pedersen, "A grip study for talk and data modes in mobile phones," *IEEE Trans. Antennas Propag.*, vol. 57, no. 4, pp. 856–865, Apr. 2009.
[29] *IEEE Standard for Safety Levels With Respect to Human Exposure to Radio Frequency Electromagnetic Fields, 3 Khz to 300 Ghz*, IEEE Standards Coordinating Committee Standard A. S. C95.1-2005, 2006.

CARLA DI PAOLA (Student Member, IEEE) received the bachelor's and master's degrees in telecommunication engineering from the University of Catania, Catania, Italy, in 2013 and 2016, respectively. She is currently pursuing the Ph.D. degree with the Antennas, Propagation, and Millimeter-Wave Systems Section, Department of Electronic Systems, Aalborg University, Aalborg, Denmark. Her current research interests include antenna design for mobile phones and OTA testing.

SAMANTHA CAPORAL DEL BARRIO was born in 1987. She received the B.Sc. degree in physics and the M.Sc. degree in telecommunication engineering and mobile communications from Grande Ecole, Paris, and the M.Sc. degrees from Paris ECE Grande Ecole and Aalborg University, in 2010. She is currently pursuing the Ph.D. degree in wireless communications with Aalborg University. After completing the scientific Classes Preparatoires aux Grandes Ecoles (CPGE), she entered a Grande Ecole, in 2005. She specialized in antennas and propagation from Aalborg University, Aalborg, Denmark. Her research interests include small terminal performances, users influence on MIMO handsets and frequency-reconfigurable antennas for 4G implementation. She is also involved in the COST Action IC 1004 on Cooperative Radio Communications for Green Smart Environments and the COST Action IC 1102 on Versatile, Integrated, and Signal-Aware Technologies for Antennas.

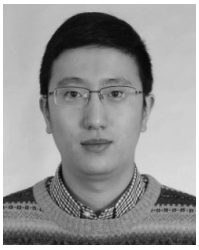

SHUAI ZHANG (Senior Member, IEEE) received the B.E. degree from the University of Electronic Science and Technology of China, Chengdu, China, in 2007, and the Ph.D. degree in electromagnetic engineering from the Royal Institute of Technology (KTH), Stockholm, Sweden, in 2013. He was a Research Fellow with KTH. In 2010, he was a Visiting Researcher with Lund University, Lund, Sweden. In 2011, he was a Visiting Researcher with Sony Mobile Communications AB, Lund. In 2014, he joined Aalborg University, Aalborg, Denmark, where he is currently an Associate Professor. From 2016 to 2017, he was also an External Antenna Specialist with Bang & Olufsen, Kongens Lyngby, Denmark. He has coauthored more than 60 articles in well-reputed international journals. He holds more than 16 (U.S. or WO) patents. His current research interests include mobile terminal mm-wave antennas, biological effects, CubeSat antennas, massive MIMO antenna arrays, UWB wind turbine blade deflection sensing, and RFID antennas.

ARTHUR S. MORRIS III (Fellow, IEEE) received the B.S. degree in physics and in electrical engineering and the M.S. and Ph.D. degrees in electrical engineering from North Carolina State University (NCSU), Raleigh, NC, USA, in 1983, 1986, and 1993, respectively. As a Scientist/Engineer with a concentration on physical electronics and electromagnetic fields for over 30 years, he has contributed to device technologies ranging from traveling-wave tubes to millimeter-wave heterojunction bipolar transistors. He has developed products for markets from high-voltage instrumentation to broadband communication systems. In 1999, he joined Coventor, to lead software and hardware development to drive the transition of microelectromechanical systems (MEMS) and microsystems from the laboratory into products for RF and optical applications. He is a cofounder of Wispry Inc., Irvine, CA, USA, which spun out of Coventor, in 2002. He is the company's Chief Technical Officer (CTO) and leads the development of high-performance programmable RF products for high-volume markets utilizing MEMS, CMOS, and advanced packaging. He is an Adjunct Professor with NCSU.

GERT FROELUND PEDERSEN (Member, IEEE) was born in 1965. He received the B.Sc. and E.E. (Hons.) degrees in electrical engineering from the College of Technology, Dublin Institute of Technology, Dublin, Ireland, in 1991, and the M.Sc.E.E. and Ph.D. degrees from Aalborg University, Aalborg, Denmark, in 1993 and 2003, respectively. Since 1993, he has been with Aalborg University, where he is currently a Full Professor heading the Antennas, Propagation and Millimeter-wave Systems Laboratory with 25 researchers. He is also the Head of the Doctoral School on Wireless Communication with some 40 Ph.D. students enrolled. He was a consultant on the development of more than 100 antennas for mobile terminals including the first internal antenna for mobile phones in 1994 with the lowest SAR, first internal triple-band antenna in 1998 with low-SAR and high-TRP and TIS, and lately various multiantenna systems rated as the most efficient on the market. He has worked most of the time with joint university and industry projects and has received more than 21 M$ in direct research funding. He is currently the Project Leader of the RANGE Project with a total budget of more than 8 M$ investigating high performance centimetre/millimetre-wave antennas for 5G mobile phones. He has been one of the pioneers in establishing over-the-air measurement systems. The measurement technique is now well established for mobile terminals with single antennas. He was the chair of various COST groups with liaison to 3GPP and CTIA for over-the-air test of MIMO terminals. He is currently involved in MIMO OTA measurement. He has authored or coauthored more than 500 peer-reviewed articles, six books, and 12 book chapters. He holds more than 50 patents. His current research interests include radio communication for mobile terminals, especially small antennas, diversity systems, propagation, and biological effects.